Phasons and broken symmetries in ferroelectric liquid crystals

I. Muševič, B. Žekš, and R. Blinc
J. Stefan Institute, Jamova 39, 61000 Ljubljana, Slovenia

Th. Rasing
Research Institute for Materials and High Field Magnet Laboratory, University of Nijmegen, NL-6525 ED Nijmegen, The Netherlands

(Received 1 December 1993)

The phason dispersion and the linear electro-optic response in the ferroelectric Sm C^* liquid-crystalline phase have been measured in an external magnetic field up to 14 T. In the presence of an external field the originally continuous phason spectrum splits into an opticlike and an acousticlike phason branch, separated by a field-dependent gap. The band structure of the phason spectrum in the presence of the field is a consequence of the broken helical symmetry of the Sm C^* phase and is analogous to the energy spectrum of an electron in a crystal lattice. The observed magnetic-field dependence of the phason spectrum is in good agreement with theory.

I. INTRODUCTION

Some time ago Blinc and Žekš[1] showed, that in the long-wavelength and low-frequency limit, the spectrum of collective excitations of the Sm C^* phase of a ferroelectric liquid crystal consists of the amplitudon and the phason dispersion branches, which merge into a doubly degenerate soft-mode branch at the Sm $A \rightarrow$Sm C^* phase-transition point. The amplitudon branch represents collective, plane-wave fluctuations of the magnitude of the tilt angle in the Sm C^* phase. It exhibits finite relaxation rates at all wave vectors and temperatures, except at the transition point T_c. The so-called phason branch of excitations represents the fluctuations of the phase of the tilt angle. In view of the continuous D_∞ symmetry of the Sm A phase, which is broken at the Sm $A \rightarrow$Sm C^* transition point, the phason branch is expected to be gapless and should thus contain a *zero frequency symmetry-restoring Goldstone mode.*[2,3] The nature of collective excitations in ferroelectric liquid crystals has been extensively studied by quasielastic light scattering[4,5] and dielectric spectroscopy[6] and is fairly well understood. For example, it has been shown that in the Sm A phase of a ferroelectric liquid crystal the soft mode freezes-out into form of a space-coherent helical wave[5] at T_c, whereas in the Sm C^* phase the experiments have confirmed the existence of a zero-frequency Goldstone mode in the phason excitation spectrum.[4]

In a recent paper[7] we have reported the magnetic-field dependence of the phason branch in the Sm C^* phase of ferroelectric liquid crystal. We observed that an external magnetic field, applied perpendicular to the helical axis of the Sm C^* phase, induces a splitting of the originally single phason branch into the so-called "acousticlike" and "opticlike" branch, respectively. These two branches are separated by a field-dependent gap $G(H)$, which is proportional to the square of the magnetic field.

The magnetic-field-induced splitting of the phason branch can be explained on the basis of pure symmetry arguments. The unperturbed Sm C^* structure is a phase with a *continuous helicoidal symmetry,* as shown by the object in Fig. 1(a). This means, that any translation of the system along the helical axis, followed by an appropriate rotation around the helical axis transforms the Sm C^* phase into itself. As a result of this continuous helicoidal symmetry, phason excitations propagate along the helical axis in a form of plane waves with a gapless dispersion relation. This can be well understood by realizing that a phason propagating along the helix is a twistlike, periodic elastic deformation of the phase profile. Since all the points on the helix are equivalent with respect to such a deformation, a phason propagating along the helix "sees" a uniformly twisted structure, which is thus equivalent to a spatially uniform structure. This results in a plane-wave phason propagation.

When an external magnetic field is applied perpendicular to the helical axis of a ferroelectric liquid crystal, molecules with positive diamagnetic anisotropy $\Delta\chi > 0$ tend to align into the field direction. As a result, the helical structure distorts in a solitonlike lattice, as shown by the object in Fig. 1(b). Large domains, where the molecules are almost completely aligned into the field direction, are separated by narrow π-domain walls, where the molecules twist rapidly over an angle π when going from one domain to the other. Here, the *continuous helicoidal symmetry* of the undisturbed Sm C^* phase *is broken* by the external field and the remaining symmetry elements are *discrete* ones. The solitonlike distorted Sm C^* phase transforms into itself by a translation along the helix by half a period $p/2$ followed by a rotation by 180° around the helical axis. Due to the presence of these π-domain walls, the phason excitation propagating along the helical axis now "feels" a periodic perturbation, which has some deep implications for the phason dynamics. In particular, the concept of a *Brillouin zone* (BZ) has to be applied, reflecting the presence of a periodic perturbation for phason propagation, which results in a *Bloch nature of phason eigenfunctions* and a *band structure of the phason excitation spectrum,* as shown in Fig. 1(d). The crossover

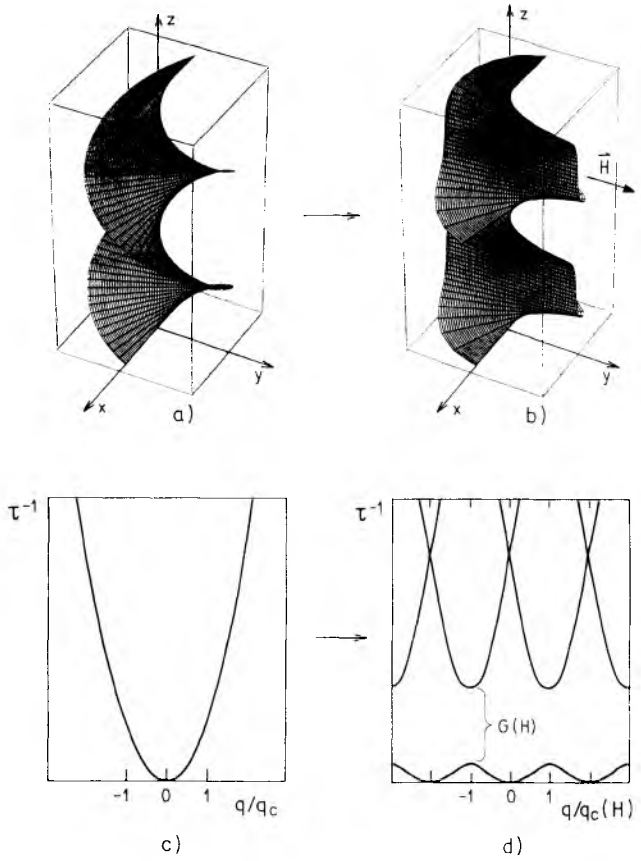

FIG. 1. The projection $\xi(z)$ of the director field on to the smectic layers for (a) $H=0$ and (b) $H\approx H_c$, as calculated from the Eqs. (1) and (3). In zero field, the unperturbed helical surface has a continuous helical symmetry as shown in (a). For $H\neq 0$ the distorted helical surface shows a discrete translational symmetry as shown in (b). (c) shows the phason dispersion in the unperturbed Sm C^* phase, whereas (d) shows schematically the phason dispersion in a solitonlike deformed Sm C^* phase.

from the plane wave to the Bloch-like phason dynamics is very similar to the crossover from the plane wave dynamics of an electron in a constant potential to the Bloch-wave dynamics of an electron in a periodic crystal lattice. Whereas in the case of phason propagation an external magnetic field breaks the continuous helicoidal symmetry of the Sm C^* phase, the presence of a periodic crystal potential breaks the continuous translational symmetry.

The aim of this paper is to present our experimental results of the magnetic-field-induced band structure of the phason excitation spectrum. We present a theoretical description of phason dynamics in an external magnetic field, which is an extension of the theoretical treatments of Sutherland,[8] Fan, Kramer, and Stephen,[9] Parsons and Hayes,[10] and Yamashita, Kimura, and Nakano.[11] We discuss the observability of the phason spectrum with quasielastic light-scattering spectroscopy and dielectric response measurements. The experimental part gives a detailed description of the high-magnetic-field experiments in the Sm C^* phase of a mixture of 35% of chiral and 65% of racemic liquid crystal 4-(2′-methylbutyl)-phenyl 4′-*n*-octylbiphenyl-4-carboxylate (CE-8 or 8SI) and presents the results of measurements that have been performed up to the highest accessible field of 14 T in the present setup.

II. THEORY

The dynamics of the Sm C^* phase of ferroelectric liquid crystals in external fields is conveniently described within the Landau thermodynamic potential,[12] where the nonequilibrium order parameter $\xi(\mathbf{r},t)$ is the projection of the long molecular axis onto the smectic planes

$$\xi_1(z,t)=\theta\cos\Phi(z,t)\ ,\quad \xi_2(z,t)=\theta\sin\Phi(z,t)\ . \tag{1}$$

We neglect the electric polarization terms and assume that the Sm C^* phase is homogeneous in the (x,y) plane. In the constant amplitude approximation the phase dependent part of the nonequilibrium free energy density $g(z,t)$ of the Sm C^* phase in an external transverse magnetic field $\mathbf{H}=(0,H,0)$ is expressed as

$$g(z,t)=-\Lambda\theta^2\frac{\partial\Phi(z,t)}{\partial z}+\tfrac{1}{2}K_3\theta^2\left[\frac{\partial\Phi(z,t)}{\partial z}\right]^2 -\tfrac{1}{2}\Delta\chi H^2\theta^2\sin\Phi(z,t)\ . \tag{2}$$

In the above expression, Λ is the coefficient of the Lifshitz term, K_3 is the torsional elastic constant, and $\Delta\chi$ is the diamagnetic anisotropy, which is assumed to be positive. The minimization of $g(z,t)$ with respect to $\Phi(z,t)$ leads to the well-known static solution $\Phi_0(z)$ of the sine-Gordon equation[12] in the form of a π-soliton lattice:

$$\sin\Phi_0(z)=\mathrm{sn}(u,k)\ . \tag{3}$$

Here $\mathrm{sn}(u,k)$ is the Jacobian sine amplitude of the argument $u=z/(\xi k)$, $\xi=\sqrt{K_3/(\Delta\chi H^2)}$ is the magnetic coherence length, and k is the modulus of Jacobian elliptic functions. It is determined by the magnitude of the external field and satisfies the equation

$$k=\frac{H}{H_c}E(k)\ ,\quad H_c=\frac{\pi^2}{p_0}\sqrt{K_3/\Delta\chi}\ . \tag{4}$$

Here, H_c is the critical magnetic field for the unwinding of the helix, $E(k)$ is the complete elliptic integral of the second kind and p_0 is the period of the helix in the unperturbed Sm C^* phase.

The nonequilibrium phase of the order parameter is written as

$$\Phi(z,t)=\Phi_0(z)+\delta\Phi(z,t)\ , \tag{5}$$

where $\delta\Phi(z,t)$ is a small fluctuating part of the phase of the order parameter. After applying the Landau-Khalatnikov equations of motion to the nonequilibrium $g(z,t)$, the fluctuating part of the phase of the order parameter is expressed as

$$\delta\Phi(z,t)=\Psi(z)e^{-t/\tau(H)}\ . \tag{6}$$

This is an overdamped phase excitation with the relaxation time $\tau(H)$, propagating along the z direction. By

linearizing the Landau-Khalatnikov equations in $\Psi(z)$, one obtains Lamé's equation of order one for the eigenvectors of the phase fluctuations amplitude $\Psi(u)$:

$$\frac{d^2\Psi}{du^2}+[h-2k^2\mathrm{sn}^2(u,k)]\Psi=0 \ . \tag{7}$$

Here $h=k^2\{\xi^2\gamma/[\tau(H)K_3]+1\}$ is the eigenvalue, which determines the relaxation time $\tau(H)$ of the excitation and γ is the rotational viscosity of the Sm C^* phase. It is interesting to note that this equation can be found in the description of the dynamics of very different physical systems, such as superconductors,[13] light propagation in periodic dielectric structures,[14] quantum theory of the band structure of solids,[8] incommensurate crystals,[15–19] and fluctuations of the order parameter in chiral nematics.[9–11]

The general solution of Lamé's equation of order one, which is in a natural way represented by a form of Bloch wave, was reported by Hermite[20] in 1872. Later on, a clear physical interpretation of the eigensolutions and eigenvalues was given by Sutherland[8] and Yamashita, Kimura, and Nakano[11] for different physical systems. The general solution $\Psi(u)$ of Lamé's equation of order one is

$$\Psi(u)\propto\frac{H(u-u_0)}{\Theta(u)}e^{-uZ(u_0)} \ , \tag{8}$$

where $H(u)$, $\Theta(u)$, and $Z(u)$ denote Jacobi's eta, theta, and zeta functions. The relaxation rate $\tau^{-1}(H)$ of the corresponding overdamped excitation is determined by the eigenvalue h of Lamé's equation and is given by

$$\tau^{-1}(H,u_0)=\frac{\Delta\chi}{\gamma}\frac{H^2}{k^2}dn^2(u_0) \ , \tag{9}$$

where $dn(u)$ is the Jacobi's δ amplitude. From Eqs. (8) and (9) one immediately observes the role of the parameter u_0. It determines the wave vector $\mathbf{q}=(0,0,q)$ of the excitation through the value of $Z(u_0)$ in Eq. (8) and the value of the relaxation rate through Eq. (9). It thus determines the dispersion relation for phason excitations and ascribes the wave vector q to the eigenfunction $\Psi_q(u)$.

Because of the translational symmetry of Lamé's equation, the eigenvalues $\Psi_q(u)$ must have the form of a Bloch wave $\Psi_q(\mathbf{r})=v_q e^{i\mathbf{qr}}$, which transforms as

$$\Psi_q(\mathbf{r}+\mathbf{R})=\Psi_q(\mathbf{r})e^{i\mathbf{qR}} \tag{10}$$

when the system is translated over a lattice vector $\mathbf{R}$. The above condition restricts the choice to pure imaginary values of $Z(u_0)$, or, what is the same:[21] $\mathrm{Re}(u_0)=n*K(k)$, $n\in Z$. Here $K(k)$ is the complete elliptic integral of the first kind, which is the quarter period of the Jacobian elliptic functions. It is connected to the magnetic-field-dependent period $p(H)$ of the helical structure

$$p(H)=p_0\left[\frac{2}{\pi}\right]^2K(k)E(k) \ . \tag{11}$$

The explicit connection between u_0 and the wave vector q can be obtained after considering the transformation properties of the eigensolution $\Psi(u)$. The magnitude of the lattice vector $|\mathbf{R}|$ is equal to $2K$, which is the period of the potential term $\mathrm{sn}^2(u)$ in the Lamé's equation, so that translational properties of the eigensolution with a wave vector q are

$$\Psi_q(u+2K)=\Psi_q(u)e^{\pm i\pi-2KZ(u_0)} \ . \tag{12}$$

Remembering that the translation over $2K$ in the reduced coordinate u also represents the translation in the z direction over $p(H)/2$, one obtains from the Eq. (12) the expression for the wave vector of the eigensolution

$$q=\mp q_c\left[1\pm i\frac{2K(k)}{\pi}Z(u_0)\right] \ . \tag{13}$$

Here we have introduced the wave vector of the Sm C^* phase, $q_c=2\pi/p$. Because of the periodic properties of the Jacobi's ζ function $Z(u+2K)=Z(u)$, relevant values of u_0 are $\mathrm{Re}(u_0)=0$ and $\mathrm{Re}(u_0)=K$. It can also be shown that these two intervals of the parameter u_0 correspond to two distinct branches of the phason excitation spectrum

$$\mathrm{Re}(u_0)=0\cdots\text{the opticlike branch} \ , \tag{14a}$$

$$\mathrm{Re}(u_0)=K\cdots\text{the acousticlike branch} \ . \tag{14b}$$

Because of the quasiperiodic properties of $Z(u)$, the analysis can be further limited to the interval: $\mathrm{Im}(u_0)\in(-K',K')$, where $K'(k)$ is the associated complete elliptic integral of the first kind. It can be shown, that this interval corresponds to the phason dispersion in *the first Brillouin zone* (BZ) and the periodic properties of Jacobi's ζ function reflect the periodic properties of the phason dispersion relation in the reciprocal space. Here the first Brillouin zone is introduced as the interval $(-q_c,q_c)$ in the reciprocal space. The introduction of the Brillouin-zone concept for director field excitations thus reflects the appearance of the periodic potential term $\mathrm{sn}^2(u)$ in the Lamé's equation, which breaks the continuous helicoidal symmetry of the undistorted Sm C^* phase.

A. The opticlike branch of the phason excitation spectrum

Let us first consider the phason-dispersion relation in the case when $\mathrm{Re}(u_0)=0$ and $\mathrm{Im}(u_0)=y_0\in(-K',K')$. The wave vector for this branch of excitations is deduced from the Eq. (13) as

$$q=\pm q_c\left\{1\pm\frac{2K(k)}{\pi}\left[Z(y_0,k')-\frac{\mathrm{sn}(y_0,k')\mathrm{dn}(y_0,k')}{\mathrm{cn}(y_0,k')}+\frac{y_0\pi}{2K(k)K'(k)}\right]\right\} , \tag{15}$$

whereas the corresponding relaxation rate is

$$\tau_+^{-1}(H)=\frac{\Delta\chi}{\gamma}\frac{H^2}{k^2}\frac{\mathrm{dn}^2(y_0,k')}{\mathrm{cn}^2(y_0,k')} \ . \tag{16}$$

Here, k' is the complementary modulus, $k'=\sqrt{1-k^2}$.

In the limit of small $y_0 \to 0$ that corresponds to the edge of the BZ [$q \to q_c$, see Eq. (15)], the dispersion relation is

$$q \to q_c : \ \tau_+^{-1}(H,q) = \frac{\Delta\chi}{\gamma}\frac{1}{k^2}H^2 + \frac{K_3}{\gamma}\frac{k^2K^2}{(E-K)^2}(q \pm q_c)^2 , \tag{17}$$

whereas the corresponding eigenfunction Ψ_q is in the form of an elliptic standing wave

$$\Psi_{q \to q_c} \propto \mathrm{sn}(u,k) , \tag{18}$$

which is characteristic for the eigensolutions at the edge of the BZ. In the vicinity of the edge of the BZ, the dispersion relation for the opticlike branch is thus parabolic and has a minimum at q_c:

$$q = q_c : \ \tau_+^{-1}(H,q_c) = \frac{\Delta\chi}{\gamma}\frac{1}{k^2}H^2 . \tag{19}$$

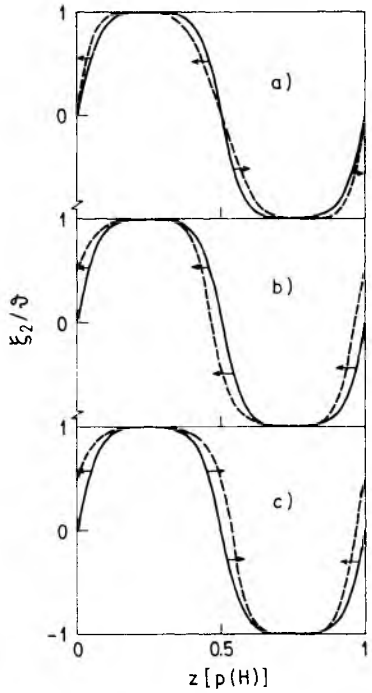

FIG. 2. The effect of the phason excitations on the order parameter ξ_2 as calculated near H_c from the Eqs. (3), (5), (18), (24), and (27). The solid lines correspond to the equilibrium phase profile $\Phi_0(z)$ whereas the effects of the phase excitations are shown by the dashed lines. (a) shows the opticlike mode at the edge of the BZ, superposed to the solitonlike deformed Sm C^* phase. This mode represents the fluctuations of the shape of π-domain walls. It is a standing, solitonlike wave with the nodes at the centers of the domains. (b) The Goldstone excitation in a solitonlike deformed Sm C^* phase. This mode represents pure translation (or the sliding) of the solitonlike lattice as a whole. (c) The acousticlike mode at the edge of the BZ, superposed to the solitonlike deformed Sm C^* phase. This mode represents coherent movement of the neighboring π-domain walls, without the change of the shape of the domain walls. It is a standing, solitonlike wave with the nodes in between the two neighboring domain walls.

The effect of such an excitation on the projection ξ_2 of the helical structure is shown in Fig. 2(a). Here, the opticlike phase excitation of the form $\Psi_q \propto \mathrm{sn}(u,k)$ has been superposed to the helical structure which is deformed in a solitonlike manner. One can clearly see, that such an excitation represents the deformation of the shape of the π-domain walls, whereas the position of domain walls remains unchanged.

The limit $\mathrm{Re}(u_0)=0$ and $\mathrm{Im}(u_0)=y_0 \to K'$ corresponds to the limit of large wave vectors, as can be seen from the Eqs. (15) and (16). Here, the phason dynamics is unaffected by the external field:

$$q \to \infty : \ \tau_+^{-1}(H,q) = \frac{K_3}{\gamma}q^2 , \ \ \Psi_q \propto e^{iqu} , \tag{20}$$

whereas the corresponding eigenfunctions Ψ_q are plane waves.

B. The acousticlike branch of the phason excitation spectrum and the Goldstone mode

The acousticlike branch of the excitation spectrum is obtained in the case $\mathrm{Re}(u_0)=K$ and $\mathrm{Im}(u_0)=y_0 \in (-K',K')$. The wave vector is deduced from the Eq. (13)

$$q = \pm q_c \left\{ 1 \pm \frac{2K(k)}{\pi} \left| Z(y_0,k') - k'^2 \frac{\mathrm{sn}(y_0,k')\mathrm{cn}(y_0,k')}{\mathrm{dn}(y_0,k')} + \frac{\pi}{2K(k)K'(k)}y_0 \right| \right\} , \tag{21}$$

whereas the corresponding relaxation rate is

$$\tau_-^{-1}(H) = \frac{\Delta\chi}{\gamma}\frac{1-k^2}{k^2}H^2\frac{\mathrm{cn}^2(y_0,k')}{\mathrm{dn}^2(y_0,k')} . \tag{22}$$

In the limit $y_0 \to K'$, which corresponds to the center of the BZ ($q \to 0$), the dispersion relation can be written from Eqs. (21) and (22)

$$q \to 0 : \ \tau_-^{-1}(H,q) = \frac{K_3}{\gamma}(1-k^2)\frac{K^2}{E^2}q^2 , \tag{23}$$

whereas the corresponding limiting eigenfunction is in a form of a standing wave

$$\Psi_{q=0} \propto \mathrm{dn}(u,k) \ \text{ and } \ \tau_-^{-1}(H,0)=0 . \tag{24}$$

Thus, for $q=0$ we get a zero-frequency (Goldstone) mode. The Goldstone excitation of the order parameter $\xi(z,t)$ as calculated near the critical field is shown in Fig. 2(b). It is interesting to note that it represents an excitation of the phase profile, which is equivalent to the translation or the sliding of the helix as a whole. Since translation costs zero energy, such an excitation has zero relaxation rate.

The parabolic phason-dispersion relation $\tau_-^{-1}(H,q)$ near the center of the BZ is strongly influenced by the external magnetic field. In particular, the corresponding restoring elastic constant $\tilde{K}_3$ is renormalized by the magnetic field

$$\tilde{K}_3 = K_3(1-k^2)\frac{K^2}{E^2} \tag{25}$$

and tends to zero near H_c. This means, that the dispersion of the acoustic branch becomes flat at the critical field H_c.

The vicinity of the edge of the BZ ($q \to q_c$) is obtained in the limit $y_0 \to 0$. The dispersion relation is then

$$q \to q_c: \quad \tau_-^{-1}(H,q) = \frac{\Delta\chi}{\gamma}\frac{1-k^2}{k^2}H^2 - \frac{K_3}{\gamma}\frac{(1-k^2)k^2K^2(k)}{[E-(1-k^2)K(k)]^2}(q \pm q_c)^2 \tag{26}$$

and the eigensolution is again in the form of an elliptic standing wave

$$\Psi_{q \to q_c} \propto \mathrm{cn}(u,k) \; . \tag{27}$$

At the edge of the BZ, the relaxation rate of the acoustic mode is thus

$$q = q_c : \quad \tau_-^{-1}(H,q_c) = \frac{\Delta\chi}{\gamma}\frac{1-k^2}{k^2}H^2 \; . \tag{28}$$

Figure 2(c) shows the acousticlike mode at the edge of the BZ, superposed to the static field-induced soliton lattice near the critical field. As one can see, this mode represents the coherent out-of-phase motion of the neighboring domain walls, whereas the shape of the domain walls remains unchanged.

C. The gap

From the Eqs. (19) and (28) we see that there are two distinct eigenvalues of the Lamé's equation of order one at the edge of the BZ. This indicates that there is a magnetic-field-induced gap

$$G(H,q_c) = \tau_+^{-1}(H,q_c) - \tau_-^{-1}(H,q_c) = \frac{\Delta\chi}{\gamma}H^2 \; , \tag{29}$$

which separates the high-frequency, opticlike excitation branch from the low-frequency, acousticlike phason branch. Magnetic-field dependencies of the relaxation rates of the opticlike and the acousticlike modes at the edge of the BZ are shown in Fig. 3, as calculated from the Eqs. (4), (19), and (28).

The spectrum of the phason excitations in a solitonlike distorted Sm C^* phase shows *only one forbidden frequency gap*. The existence of a single forbidden frequency gap is here related to the particular form of the potential in the Lamé's equation, $V \propto \mathrm{sn}^2(u,k)$ and is in sharp contrast to the band structure of three-dimensional (3D) solids, where usually a large number of gaps exist.

The dispersion relation for the phase excitations, propagating along the helical axis of the Sm C^* phase, distorted by a transversal magnetic field, is shown in Fig. 4. The dispersion was calculated for different field strengths from the Eqs. (4), (11), (15), (16), (21), and (22). Figure 5 shows a 3D view of the phason dispersion surface $\tau^{-1}(H,q)$ in the region $0 \le q \le 2q_c$ and $0 \le H \le H_c$. One

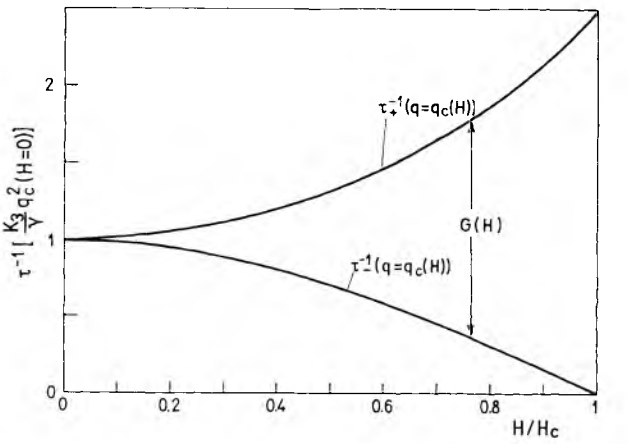

FIG. 3. The splitting of the phason mode at the edge of the Brillouin zone, calculated according to the Eqs. (4), (19), and (29).

can observe the evolution of a band gap $G(H)$ at the edge of the zone, together with a shrinking of the size of the BZ, which is a result of the magnetic-field dependence of the period of the helical structure [Eq. (11)]. At the critical magnetic field, the Brillouin zone shrinks to a single Goldstone mode at $q = 0$, which disappears at H_c. Above the critical field, only one parabolic dispersion branch evolves from the opticlike phason branch

$$H \ge H_c : \quad \tau^{-1}(H,q) = \frac{K_3}{\gamma}q^2 + \frac{\Delta\chi}{\gamma}H^2 \; , \tag{30}$$

which has a finite gap $(\Delta\chi/\gamma)H^2$.

D. The role of a small transverse component of the wave vector

Due to the experimental restrictions in a light-scattering experiment, one usually observes phase excitations with a wave vector $\mathbf{q} = (q_x, 0, q_z)$, propagating at a small angle with respect to the helix. The phason disper-

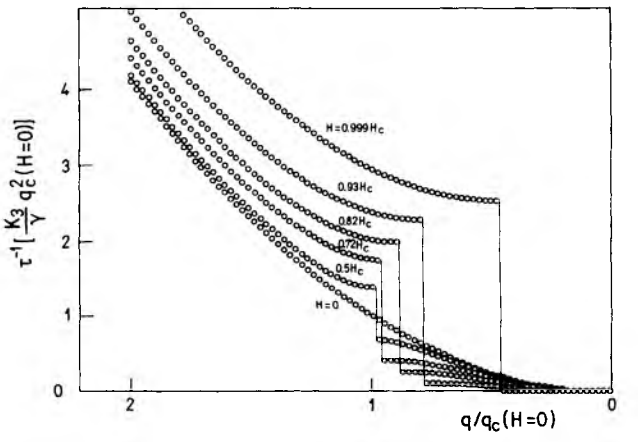

FIG. 4. Phason dispersion, as calculated from the Eqs. (4), (11), (15), (16), (21), and (22) at different magnetic fields.

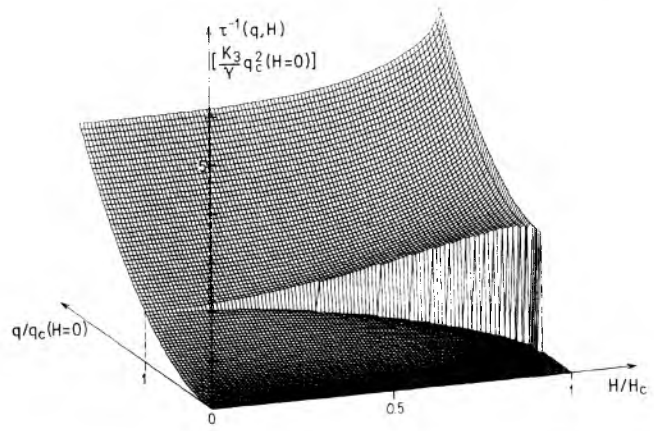

FIG. 5. 3D view of a calculated phason dispersion $\tau^{-1}(q,H)$ as a function of an external field. Note the appearance of a gap near q_c already at very small fields. Because of the numerical discreteness in H, the shrinking of the BZ near H_c is not complete.

sion for oblique propagation was considered recently[5] and it was found that the transverse component of the wave vector induces a splitting of the phason branch even in the absence of external fields. In order to elucidate the influence of the external magnetic field on the band gap in this situation, one obtains after an analysis similar to Ref. 5 an equation, describing the dynamics of phase excitations, propagating at a small angle with respect to the helix

$$\frac{d^2\Psi}{du^2}+[h-2k^2\mathrm{sn}^2(u,k)]\Psi - \frac{k^2}{\Delta\chi H^2}[K_1\mathrm{sn}^2(u,k)+K_2\mathrm{cn}^2(u,k)]q_x^2\Psi=0 \ . \quad (31)$$

Here K_1 and K_2 are splay and bend elastic constants for the 2D nematic field, respectively. In the limit of small q_x, one obtains a first-order correction to the dispersion relation for phasons, propagating at small angles to the helical axis

$$\tau^{-1}(\mathbf{q},H)=\tau^{-1}(q_z,H) + \frac{1}{\gamma}\frac{\langle\Psi_q|K_1\mathrm{sn}^2(u,k)+K_2\mathrm{cn}^2(u,k)|\Psi_q\rangle}{\langle\Psi_q|\Psi_q\rangle}q_x^2 =\tau^{-1}(q_z,H)+\frac{K_x}{\gamma}q_x^2 \ . \quad (32)$$

Here $|\Psi_q\rangle$ denotes the eigensolution of the unperturbed Lamé equation with the wave vector $\mathbf{q}=(0,0,q_z)$, $\tau^{-1}(q_z,H)$ is the corresponding relaxation rate, whereas

$$\langle\Psi|f|\Psi\rangle=\int\Psi^*(z)f(z)\Psi(z)dz \ .$$

From the above expression one can see that the correction to the eigenvalue is always positive and removes the degeneracy of the eigensolutions even in zero field. The magnitude of the correction term depends on the normalized, space-averaged value of the combination of splay and bend elastic constants and can be easily evaluated at the edge and in the center of the BZ, where the eigenfunctions obtain simple form $\mathrm{sn}(u,k)$, $\mathrm{cn}(u,k)$, and $\mathrm{dn}(u,k)$, respectively. By taking $K_1/K_2\approx4$,[22] one obtains at zero magnetic field a splitting of the order of $\Delta(q_x)\approx0.4K_1q_x^2$ at the edge of the BZ. The influence of external magnetic field on the correction term is small. It can be shown that at the edge of the BZ and near H_c, the relaxation rates of both modes increase slightly ($\approx0.07K_1q_x^2$ increase up to the critical field), whereas near the center of the BZ a decrease of similar order is expected. As a consequence, the magnetic-field dependence of the magnitude of the band gap is only slightly perturbed by the presence of the q_x component. In the experiment, this perturbation is less than 100 Hz in comparison to the phason relaxation rates of ≈1.5 kHz.

III. OBSERVABILITY OF PHASON DYNAMICS

A. The wave vector of the phason excitation

In an experiment, such as quasielastic light scattering or dielectric response, one observes the excitations of the order parameter, and not directly the excitations of the phase of the order parameter. This has the consequence, that the wave vector, ascribed to a particular eigensolution of the equation for the amplitude of the phase of the order parameter [Eq. (7)], is different from the wave vector, ascribed to the excitation of the order parameter ξ. This can be easily seen from the ξ_1 component of the order parameter, which is in the limit of small phase excitations

$$\xi_1=\mathrm{cn}(u,k)-\Psi_q(u,k)\mathrm{sn}(u,k)e^{-t/\tau(H,q)} \ . \quad (33)$$

Here $\Psi_q(u,k)$ is the eigensolution in a form of a Bloch wave $\Psi_q=p_qe^{iqz}$. After expanding $\mathrm{sn}(u,k)$ in plane waves, one obtains ξ_1

$$\xi_1=\mathrm{cn}(u,k)+(w_{q+q_c}e^{i(q+q_c)z} +v_{q-q_c}e^{i(q-q_c)z})e^{-t/\tau} \ , \quad (34)$$

where w_{q+q_c} and v_{q-q_c} are functions with a period $2K(k)$. From the Eq. (34) we see, that the excitation of the phase of the order parameter with the wave vector $\mathbf{q}$ and relaxation rate $\tau^{-1}(H,\mathbf{q})$ is observable as an excitation of the order parameter with the wave vector $\mathbf{Q}=\mathbf{q}\pm\mathbf{q}_c$ where $\mathbf{q}_c=(0,0,q_c)$. This means, that the Brillouin zone of the observable ξ_1 is shifted by $\pm\mathbf{q}_c$ in the reciprocal space. This has the consequence, that, for example, in a light-scattering experiment, the Goldstone mode is observable near the critical wave vector $\mathbf{q}_c$, i.e., near the Bragg diffraction peak. Consequently, the band gap should be observable at zero scattering wave vector $\mathbf{q}_s=\mathbf{0}$.

It should be stressed, that in the literature one encounters very often rather loose use of the expression "the Goldstone mode." This is in particular true for many dielectric measurements, reporting the observation

of the Goldstone mode contribution to the dielectric response. In a dielectric experiment, the response of the system to the homogeneous ($\mathbf{Q}=\mathbf{0}$) external field is measured. As it can be seen from Eq. (34), the probing field with $\mathbf{Q}=\mathbf{q}\pm\mathbf{q}_c=\mathbf{0}$ couples to the phason mode with $\mathbf{q}=\pm\mathbf{q}_c$, thus measuring the response of the modes at the edge of the BZ, i.e., the acoustic or the opticlike mode. The true Goldstone mode, which is a zero-frequency, symmetry-restoring mode, is of course not observable in a dielectric experiment in a helicoidal structure. It is accessible only in a light-scattering experiment, where the wave vector of the excitation under observation is selected with the proper choice of the scattering wave vector.

B. Quasielastic light scattering on the phase fluctuations

Light scattering in spatially modulated, birefringent Sm C^* is treated in the Born approximation and the Sm C^* phase is considered as an optically uniaxial crystal. The eigenwaves of light propagation are thus linearly polarized ordinary $|\mathbf{k},\sigma\rangle$ and extraordinary $|\mathbf{k}',\pi\rangle$ waves with the wave vectors $\mathbf{k}$ and $\mathbf{k}'$ and polarizations σ and π, respectively. This approximation is valid at small values of the tilt angle θ when the inhomogeneous part of the dielectric tensor is a small perturbation. It breaks down in the case of the degeneration of the eigenwaves,[23] which includes the light propagation along the helical axis and the propagation at a Bragg angle.

In a ferroelectric smectic liquid crystal, the excitations of the order parameter $\delta\xi(\mathbf{r},t)$ are strongly coupled to the excitations of the dielectric tensor $\delta\underline{\epsilon}(\mathbf{r},t)$. As a result, light is scattered by thermally excited order-parameter fluctuations and this scattering can be easily observed and analyzed with the quasielastic light-scattering technique. For example, an excitation of the order parameter $\delta\xi(z,t)$ results in fluctuations of the dielectric tensor components[5]

$$\delta\underline{\epsilon}_{xz}(z,t)\propto\xi_1(z,t)\ ,\quad \delta\underline{\epsilon}_{yz}(z,t)\propto\xi_2(z,t) \tag{35}$$

and leads to a strong, depolarized scattering between the $|\mathbf{k},\sigma\rangle$ and $|\mathbf{k},\pi\rangle$ waves. In the Born approximation the corresponding autocorrelation function of the scattered light intensity is proportional to the autocorrelation function of the phase excitation $\Psi_q(z,t)$. The geometrical scattering cross sections for the optic and the acoustic modes are comparable in magnitude and do not depend strongly on the magnitude of the field except very near H_c. The difference in the magnitude of the scattering cross sections is introduced only through the mean square of the thermal amplitudes of both modes, which is in favor of the lower-frequency acoustic modes.

C. Linear electro-optic response

Whereas the quasielastic light-scattering spectroscopy allows for the determination of the dispersion relation for the order-parameter excitations, dielectric spectroscopy is a very useful probe for determining the susceptibilities of the soft, amplitude, and phase modes at $\mathbf{Q}=\mathbf{0}$. In contrast to the optical spectroscopy, dielectric spectroscopy suffers an inherent deficiency of probing rather thin, bookshelf-aligned samples with a large surface area. Such a restricted planar geometry can, in principle, lead to the surface-induced band structure of phason excitations via the surface-induced deformation of the helical structure. In order to minimize the surface effects, it is appropriate to use the homeotropic geometry of the sample, where the classical dielectric detection technique cannot be applied. This problem can be circumvented by an optical detection technique[24] of the linear response of the Sm C^* phase to a small external electric field. A small in-plane external electric field $\mathbf{E}_0e^{i\omega t}$ is applied to the undistorted Sm C^* phase in a homeotropic geometry. It couples linearly to the spontaneous polarization $\mathbf{P}$ and induces a small phase distortion $\delta\phi(z,t)$ with the amplitude[6]

$$\delta\phi_0(z)\propto\frac{1}{1+i(\omega\gamma/K_3q_c^2)}\sin(q_cz)\ . \tag{36}$$

The electric field thus couples to the phason mode with the wave vector q_c at the edge of the Brillouin zone. This phase distortion results in the distortion of the dielectric tensor at optical frequencies, which corresponds to a small tilting of the optical axis of the Sm C^* phase in a plane, perpendicular to the direction of the applied field. Electric-field-induced tilt of the Sm C^* optical axis can be easily detected with optical conoscopy. From the frequency dependence of this linear electro-optic response one can determine the relaxation rate $(K_3/\gamma)q_c^2$ of the phason mode at the edge of the BZ.

The situation is somewhat different in a distorted helicoidal structure. First, the single mode at the edge of the BZ splits into an acoustic and opticlike mode, and second, in view of the periodicity of the phason-dispersion relation, an infinite number of higher-frequency opticlike modes should appear at the edge of the BZ. Nevertheless, the relaxation frequency of the opticlike mode, originating from the second BZ is typically an order of magnitude higher than the relaxation frequency of the two lowest modes and can be neglected.

The contributions of the acoustic and lowest lying opticlike mode to the electro-optic response of a distorted helicoidal structure can be calculated from the free-energy density, which includes the electric polarization terms.[6] This analysis can be simplified by considering the electric polarization properties of the phason excitations at the edge of the BZ. By remembering that any excitation of the director field $\delta\xi(z,t)$ is also an excitation of the polarization field $\delta\mathbf{P}(z,t)$, the relation between the fluctuations of the polarization field and the director field can be obtained from the free-energy expansion[6] as

$$\delta P_x=\epsilon\mu\frac{d\delta\xi_x}{dz}-\epsilon C\delta\xi_y\ , \tag{37a}$$

$$\delta P_y=\epsilon\mu\frac{d\delta\xi_y}{dz}+\epsilon C\delta\xi_x\ . \tag{37b}$$

Here μ and C are the flexo- and piezoelastic coefficients and ϵ is the high-frequency dielectric constant of the Sm A phase. In the limit of small fields, the response of the Sm C^* structure to the spatially homogeneous external

electric field is determined by the coupling of the field to the phason excitations, which represent space homogeneous fluctuations ($\mathbf{Q}=\mathbf{0}$) of the electric polarization field. For the two modes at the edge of the BZ we obtain the space-averaged polarization $\langle \mathbf{P} \rangle$ (or the space-homogeneous polarization):

The acousticlike mode: $\langle \delta P_x \rangle \propto \epsilon C \langle \mathrm{cn}^2(u,k) \rangle \neq 0$, (38a)

$$\langle \delta P_y \rangle = 0 , \tag{38b}$$

The opticlike mode: $\langle \delta P_x \rangle = 0$, (39a)

$$\langle \delta P_y \rangle \propto \epsilon C \langle \mathrm{sn}^2(u,k) \rangle \neq 0 . \tag{39b}$$

For the magnetic field applied in the y direction, the acoustic mode represents a collective excitation with a space homogeneous polarization $\langle \mathbf{P} \rangle \perp \mathbf{H}$, whereas for the optic mode the polarization is $\langle \mathbf{P} \rangle \| \mathbf{H}$. The above relations thus enable selective probing of the optic or the acousticlike mode via the polarization-selection rules .

IV. EXPERIMENT

The quasielastic light scattering and electro-optic response of the Sm C^* phase in a transverse magnetic field were measured in a setup, fitting into the 60-mm bore of a Bitter magnet. The geometry of the quasielastic light-scattering experiment is shown in Fig. 6. He-Ne laser light was expanded via L_1 and L_2 to a 6-mm-diam beam and then slightly focused to ≈ 100 μm spot in the liquid crystalline sample (S), placed in a thermostated oven (OV) in the center of a Bitter magnet (BM). A system of adjustable miniature Al mirrors AM_1 and AM_2 was used for fine alignment of the beam. The polarization of the incoming beam was selected by the polarizer POL, whereas the incidence angle was defined by the rotation of the sample around the direction of the field. The scattered light in the quasielastic light-scattering experiment or the transmitted light in the electro-optic measurements were collected with an optical system formed by an adjustable mirror AM_3, pinhole (PIN1), lens (L_3), analyzer (AN), tilted mirror with a pinhole (M_4), and an eyepiece (EY). The collecting optics was mounted on a rotatable arm and was fine aligned to the illuminated spot with the mirror AM_3. The scattering plane of the experiment was thus perpendicular to the direction of the magnetic field.

The illuminated spot was observed with the lens L_3 and the eyepiece EY and was fine aligned to the ≈ 100-μm pinhole in the tilted mirror by translating the lens L_3. After inserting the pinhole PIN1, the scattered light from less then one coherence area was transmitted through the pinhole in the tilted mirror and captured into a multimode fiber (F). The collected light was led to the photomultiplier (PMT), placed far away from the magnet and connected to the photon counting unit and the digital clipped autocorrelator.

In the measurements of the electro-optic response, the light intensity, transmitted through the sample placed between crossed polarizers was detected. The polarization of the light was set at 45° to the scattering plane, whereas the angle between the sample normal and the light direction was set to the half-intensity point of the conoscopic figure. The probing electric field was applied in the direction of the magnetic field, and the magnitude and the phase of the transmitted light intensity was detected with a lock-in amplifier.

Besides the light-scattering and linear electro-optic response measurements, the magnetic-field dependence of the period of the helix was determined from the Bragg diffracted peaks. As shown by Garoff, Meyer, and Barakat,[25] the Bragg diffraction peak can be observed as strong *static depolarized scattering in the forward direction* in a homeotropic sample with sufficiently long period of the helix. This depolarized, forward scattered peak was indeed observed by recording the angular depen-

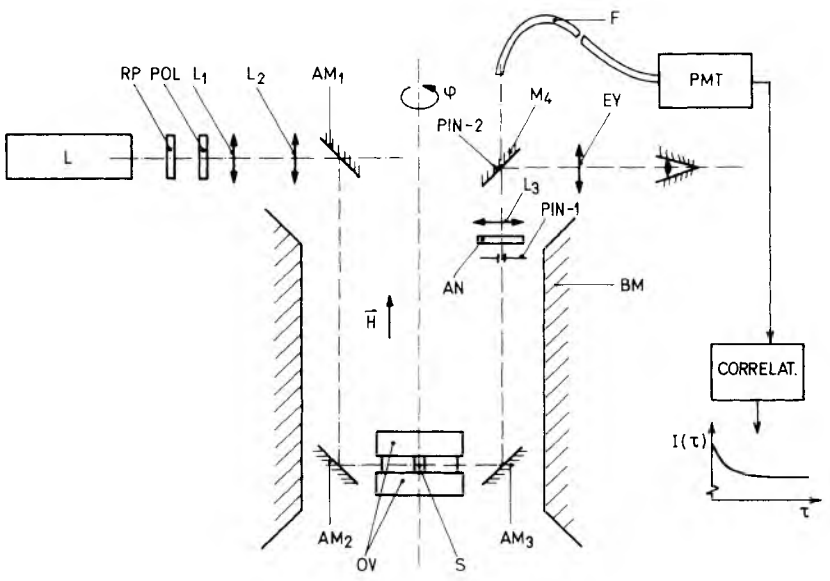

FIG. 6. The setup. Definitions: L, laser; RP, polarization rotator; Pol, polarizer; L_1, L_2, L_3, lenses; AM_1, AM_2, AM_3, adjustable mirrors; OV, oven; S, sample; PIN-1, PIN-2, pinholes; AN, analyzer; M_4 mirror; EY, eyepiece, F, fiber; PMT, photomultiplier; BM Bitter magnet.

dence of the transmitted light with ordinary incident and extraordinary outgoing polarizations or vice versa.

A mixture, consisting of 35% of pure chiral liquid crystal 4-(2'-methylbutyl)phenyl 4'-*n*-octylbiphenyl-4-carboxylate (CE-8 or 8SI) and 65% of racemic liquid crystal CE-8R was studied in the experiment. In view of the rather large period of the helix in this mixture, the critical field for helix unwinding was well below the highest accessible value of 14 T. Homeotropic aligned samples of 120 μm thickness were prepared between two clean glass plates, treated with dimethyloctadecyl-3-(trimethoxysilyl)propylammonium chloride. In some samples, two copper wires were added for the electrooptic response measurements. The quality of the alignment was carefully checked and only defect-free samples were used in the experiment.

Because of rather poor temperature stability (± 0.1 K) of the setup, the experiment was performed 3 K below the Sm $A \rightarrow$Sm C^* transition point. The measurements were performed by slowly increasing the magnetic field in steps of 0.1–0.2 T, followed by 5–10 min intervals to reach the new equilibrium state. The evolution towards the new equilibrium was clearly observable from the time evolution of the values of the measured phason relaxation times and the scattered light intensity. The response of the sample was qualitatively different in the vicinity of the critical field for the helix unwinding. Here, the system response to a 0.1-T step did not settle down even after 10 min, indicating a very slow unwinding process of the Sm C^* phase. In some samples, a very peculiar behavior of the sample was observed near H_c. When observing the illuminated spot through the eyepiece, a small increase of the field was accompanied by periodic changes of the intensity of the illuminated spot that persisted for minutes. The period of this "strobing" was of the order of a second. Beyond the critical field, the equilibrium was relatively quickly achieved. These observations lead to the conclusion, that measurements of the dynamics of the helicoidal phases in external fields should be performed very carefully and slowly, thus assuring that the system settles in the equilibrium state.

Quasielastic light-scattering measurements were performed with the incoming ordinary and the scattered extraordinary polarizations. The small angle (≈ 1 deg) of the collecting optics with respect to the transmitted beam assured that the quasielastic light-scattering experiment was always in the heterodyne regime due to the parasitic elastic scattering from the imperfections in the sample. The scattering wave vector $\mathbf{q}_s$ was calculated from the optically uniaxial model of the Sm C^* phase and has in this geometry a small transverse component. This assures that the very vicinity of the Bragg peak is avoided and introduces a small correction to the phason relaxation rates. All the data on the phason dispersions were correspondingly corrected with respect to this small transverse component. Below the critical magnetic field, the signal-to-noise ratio of the measured autocorrelation function of the scattered light intensity in the Sm C^* phase was always better than 10^2:1, which allowed for the detailed analysis of the observed signal. In contrast to our previous measurements of the phason dispersion in helicoidal phases,[4,5] which were performed in the vicinity of the Sm $A \rightarrow$Sm C^* transition, the observed autocorrelation function could clearly not be fitted to a single exponential decay function. A very good fit was obtained with a two exponential decay function, where the intensity of the low relaxation rate signal was several times larger than the magnitude of the high relaxation rate signal. Measurements of the dispersion relations for both relaxation rates revealed the origin of the spurious high-frequency signal. Whereas the dispersion minimum for the low relaxation rate signal coincided with the position of the first Bragg peak ($\mathbf{q}_s = \mathbf{q}_c$), the minimum of the dispersion of the high-frequency signal was at the position of the second Bragg peak ($\mathbf{q}_s = 2\mathbf{q}_c$), which is observable at these temperatures. The reason for this peculiar behavior is in the very specific form of the dielectric tensor $\underline{\epsilon}(\mathbf{r})$ of the Sm C^* phase which has two Fourier components $\underline{\epsilon}(q_c)$ and $\underline{\epsilon}(2q_c)$.[25] Very near T_c, where the tilt angle is small, the $\underline{\epsilon}(q_c)$ component is dominant, because it is proportional to the tilt angle, whereas the $\underline{\epsilon}(2q_c)$ component is negligible, since it is proportional to the square of the tilt angle.[25] By lowering the temperature, the tilt angle increases and the component $\underline{\epsilon}(2q_c)$ becomes more important and contributes to the scattering cross section, which explains the observed two-exponential decay. The presumption that the origin of the two-exponential decay is in the peculiar form of the dielectric tensor of the helicoidal structure is further supported by the one-exponential decay function obtained beyond the critical field, where the phase is spatially homogeneous. On the basis of the observed dispersion relations, we concluded that the low relaxation rate signal can be attributed to the acousticlike phason modes. The contribution of the opticlike phason modes, which is expected to be small because of their high relaxation rate, is covered by the above mentioned spurious signal and cannot be resolved. It is only observed as a small signal above the critical field, where the low-frequency signal from the acousticlike modes disappears.

V. RESULTS AND DISCUSSION

Dispersion relations for the acousticlike phason branch as obtained at different field strengths are shown in Figs. 7(a)–7(d), respectively. Below the critical field H_c [Figs. 7(a)–7(c)], one can clearly see that the center of the dispersion relation shifts to smaller wave vectors upon increasing magnetic field. This is consistent with the expected increase of the helical pitch and consequent decrease of the width of the BZ. At the critical magnetic field, the signal from the acousticlike phason modes disappears and a sudden abrupt change from $\tau^{-1}(\mathbf{Q}=0) \approx 800$ Hz to $\tau^{-1}(\mathbf{Q}=0) \approx 3000$ Hz is observed [Fig. 7(d)]. The dispersion becomes centered at $Q_z = 0$, which indicates that the signal originates from the opticlike phase fluctuations in the unwound, spatially homogeneous Sm C phase. This is furthermore confirmed by the gradual increase of the phason relaxation rates upon increasing magnetic field, which is in agreement with theoretical predictions.

The observed dispersions were fitted to a simple parabolic dependence $\tau^{-1}=[\tilde{K}_3(H)/\gamma][Q_z-q_c(H)]^2$, where $\tilde{K}_3(H)=K_3(1-k^2)(K^2/E^2)$ is the magnetic field renormalized torsional elastic constant. This approximation is valid only near the bottom of the acousticlike phason branch and breaks down near the edges of the BZ. The results of the fitting procedure with $\tilde{K}_3(H)$ and $q_c(H)$ as the fitting parameters, are listed in Table I, together with theoretical estimates for $H_c=8$ T. Here we obtain zero-field value $K_3/\gamma=1.13\times10^3\ \mu m^2\,s^{-1}$, which is comparable to the values, obtained in pure CE-8.[5]

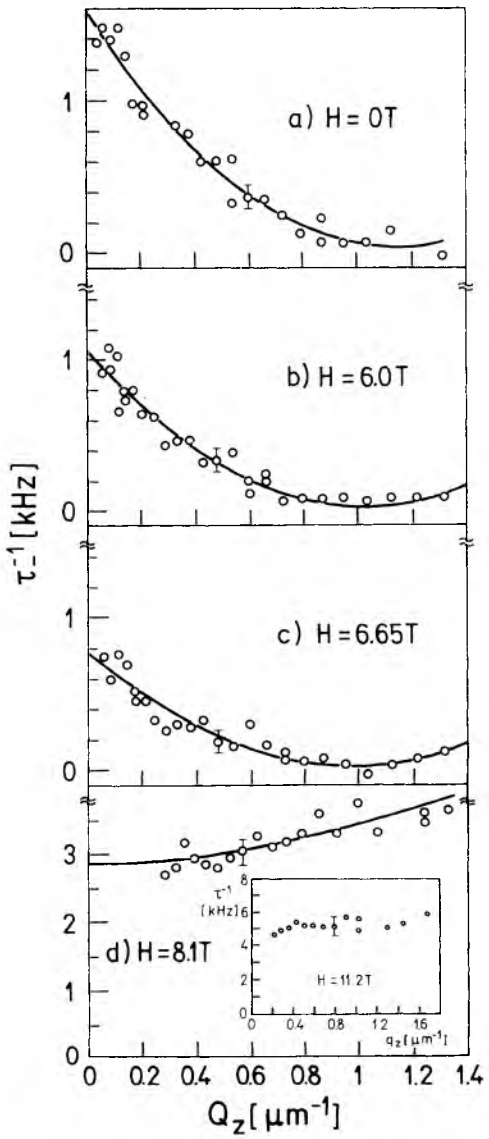

FIG. 7. Dispersion of the acousticlike phason branch at different magnetic fields. Solid lines represent the best parabolic fit $\tau^{-1}=(\tilde{K}_3/\gamma)[Q_z-q_c(H)]^2$ with (a) $\tilde{K}_3/\gamma=1.1\times10^3\ \mu m^2 s^{-1}$ and $p_0=5.7\ \mu$m at $H=0$, (b) $\tilde{K}_3/\gamma=0.97\times10^3\ \mu m^2\,s^{-1}$ and $p=6.0\ \mu$m at $H=6.05$ T, (c) $\tilde{K}_3/\gamma=0.76\times10^3\ \mu m\,s^{-1}$ and $p=6.2\ \mu$m at $H=6.65$ T and (d) $\tilde{K}_3/\gamma=0.6\times10^3\ \mu m^2\,s^{-1}$ and $q_c=0$ at $H=8.1$ T. The inset to (d) shows the phason dispersion at 11.2 T.

TABLE I. Results of the fitting procedure with $\tilde{K}_3(H)$ and $q_c(H)$ as the fitting parameters together with theoretical estimates for $H_c=8$ T.

	$\tilde{K}_3(H\neq0)/K_3(H=0)$		$p(H\neq0)/p(H=0)$	
H/H_c	Theory	Exp.	Theory	Exp.
0	1	1	1	1
0.75	0.75	0.85±0.09	1.07	1.05±0.07
0.83	0.61	0.67±0.07	1.13	1.08±0.07

As one can see from Table I, the agreement with the theoretically predicted values is good within the experimental accuracy and clearly shows the "flattening" of the acousticlike phason branch upon increasing magnetic field. Beyond the critical magnetic field the phason dispersion could not be determined very accurately because of the decreased s/n ratio of the signal of the phason branch and the increase of the relaxation rates with increasing magnetic field. This results in a rather large absolute error (≈1 kHz at 14 T) of the relaxation rates, which is comparable with the overall magnitude of the phason dispersion in the angle of accessible wave vectors. Whereas the above results confirm the theoretically predicted flattening of the acousticlike phason branch, the behavior of the opticlike phason mode at $Q_z=0$ was probed by the frequency dependence of the linear electro-optic response in the geometry $\mathbf{E}\|\mathbf{H}\perp\mathbf{q}_c$. The observed frequency dependence of the response in the range 100 Hz to 100 kHz was fitted to Eq. (36) with the relaxation rate $\tau^{-1}(\mathbf{Q}=\mathbf{0})=(K_3/\gamma)q_c$ as a fitting parameter. In contrast to the observed decrease of the relaxation rates of the acousticlike phason modes, an increase of the relaxation rates upon increasing magnetic field was observed for the opticlike modes in the linear-response measurements.

Normalized relaxation rates of both acoustic- and opticlike phason modes at $\mathbf{Q}=\mathbf{0}$, as determined from the quasielastic light-scattering and linear-response measurements are shown in Fig. 8(a) together with the period of the helix in Fig. 8(b). One can clearly see the band gap $G(H)$ emerging in between the optic- and acousticlike phason branches. By comparing the magnetic-field dependence of both relaxation rates with the magnetic-field dependence of the period of the helix, one observes a striking difference. Whereas the period of the helix is almost not influenced up to 6 T, both relaxation rates change considerably already at very small fields. Both magnetic-field dependencies were fitted to the Eqs. (19) and (28), shown as a solid line in Fig. 8(a). The fit yields $\Delta\chi/\gamma=42\ T^{-2}s^{-1}$ and $H_c=9.7$ T for the acousticlike branch in comparison to $\Delta\chi/\gamma=48\ T^{-2}s^{-1}$ and $H_c=8.1$ T for the opticlike branch. Whereas the $\Delta\chi/\gamma$ values are very close, the discrepancy in the critical fields is attributed to the fact that the measurements were done in different samples with slightly different periods p_0 of the helix. Since zero-field phason relaxation rates at $\mathbf{Q}=\mathbf{0}$ are proportional to p_0^{-2}, this also explains a small difference in the zero-field relaxation rates of the acousticlike mode (1.6±0.2 kHz) and the opticlike mode

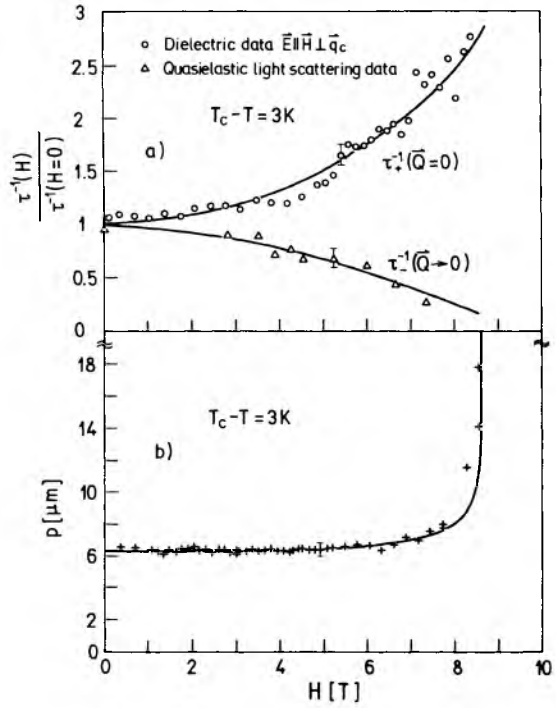

FIG. 8. Magnetic-field dependence of the (a) normalized relaxation rates of the optic and acoustic phason mode at $\mathbf{Q}=0$ and (b) period of the helix. Solid lines in (a) represent the best fits by Eqs. (19) and (29) with $\Delta\chi/\gamma=48\ \mathrm{T}^{-2}\mathrm{s}^{-1}$ and $H_c=8.1$ T for the optic phason mode $\tau_+^{-1}(0)$ and $\Delta\chi/\gamma=42\ \mathrm{T}^{-2}\mathrm{s}^{-1}$ and $H_c=9.7$ T for the acoustic phason mode $\tau_-^{-1}(0)$. The solid line in (b) represents the constant amplitude approximation fit by Eq. (11) with $p_0=6.2\ \mu$m and $H_c=8.6$ T.

(1.4±0.2 kHz).

The magnetic-field dependence of the band gap, separating the acousticlike and the opticlike phason branch at $\mathbf{Q}=0$ is shown in Fig. 9 up to the highest accessible field of 14 T. Here, for the last two points at 11.2 and 14 T, an average value of the phason relaxation rates

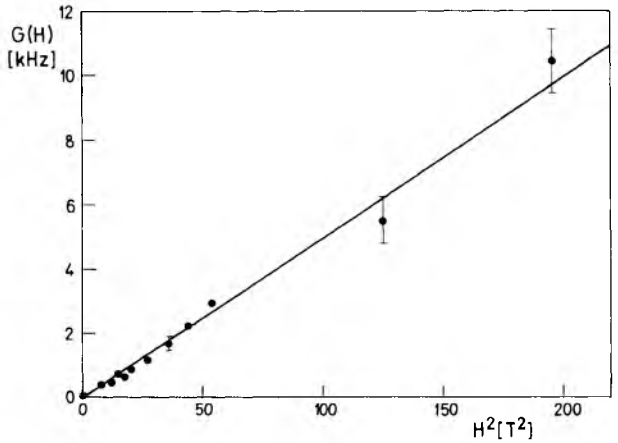

FIG. 9. Magnetic-field dependence of the gap $G(H)$, separating the optic and acoustic phason modes at $\mathbf{Q}=0$, $T_c-T=3$ K as determined up to 14 T. The difference between the normalized optic and acoustic phason relaxation rates was multiplied by the mean value of 1.5 kHz for both relaxation rates at zero field to obtain $G(H)$.

in the measuring range $0.1\ \mu\mathrm{m}^{-1}\le Q_z\le 1.2\ \mu\mathrm{m}^{-1}$ was taken. The solid line in Fig. 9 represents the best fit of measured $G(H)$ to Eq. (30) and yields $\Delta\chi/\gamma=50\ \mathrm{T}^{-2}\mathrm{s}^{-1}$, which is in very good agreement with the $\Delta\chi/\gamma$ values, as obtained from the data in Fig. 8. From the measured values of $K_3/\gamma=1.1\times10^3\ \mu\mathrm{m}^2\mathrm{s}^{-1}$ and $\Delta\chi/\gamma=50\ \mathrm{T}^{-2}\ \mathrm{s}^{-1}$ we obtain $K_3/\Delta\chi=22T^2\ \mu\mathrm{m}^2$. This is in very good agreement with the value $K_3/\Delta\chi\approx21T^2\ \mu\mathrm{m}^2$, as obtained from the expression for the critical magnetic field [Eq. (4)], where $H_c\approx8$ T and $p_0=5.7\ \mu$m. We may thus conclude that the consistency of the experimental data is very good.

Finally, we would like to extend the discussion of magnetic-field-induced phason band structure to the influence of an external electric field on the spectrum of phase excitations by using simple symmetry arguments. Although treated previously,[26] there is still a lack of a clear physical interpretation, which would elucidate rather inconsistent experimental data.[27,28] It can be shown[29] that in the presence of the ferroelectric coupling term $-\mathbf{P}\cdot\mathbf{E}$, the Landau-Khalatnikov equation, describing the propagation of phase excitations with wave vector $\mathbf{q}=(0,0,q)$ is essentially the Lamé's equation of order one. Therefore, the analysis of the eigenfunctions and eigenvalues is similar to the magnetic-field case, with one fundamental difference. Whereas the period of the $\mathrm{sn}^2(u,k)$ term in the Lamé's equation is equal to $p(H)/2$ in the case of magnetic-field coupling, it equals $p(H)$ in the case of the linear ferroelectric coupling. This has an important implication on the size of the BZ and on the location of the electric-field-induced gap. As we have shown, the size of the BZ in the magnetic-field case is $-q_c\le q\le q_c$ and the band gap is observable at $\mathbf{Q}=0$ in the laboratory system, as shown in Fig. 10(a). In view of the twice as large periodicity of the potential term in the case of ferroelectric coupling, the corresponding BZ is $q_c/2\le q\le q_c/2$ and the band gap appears at $Q_z=q_c/2$ in the laboratory system, as shown in Fig. 10(b). The electric-field-induced band gap is thus observable only in the light-scattering experiment and cannot be observed with dielectric spectroscopy. Nevertheless, some specific changes of the phason relaxation rate should be observable in a dielectric experiment. A simple estimation of the electric-field effect on the lowest-lying phason mode at $\mathbf{Q}=0$ reveals that its relaxation rate is nearly field-independent up to the vicinity of the critical field where it drops for approximately 20%, as shown schematically in Fig. 10(d). This is in sharp contrast with the reported dielectric experiments, where usually a monotonous increase of the relaxation is observed upon increasing electric field. The exception is the experiment where the optical detection method was used[27] and a nonmonotonous field dependence of the relaxation rate, resembling the one expected, was observed near the critical electric field. We believe, that in these experiments, the geometry and the strong influence of the surface anchoring plays a major role. An experiment with the biasing electric field in a homeotropic geometry and using the optical detection technique would probably reveal the true phason dynamics, unperturbed by the surface anchoring.

We conclude the discussion of the phason dynamics

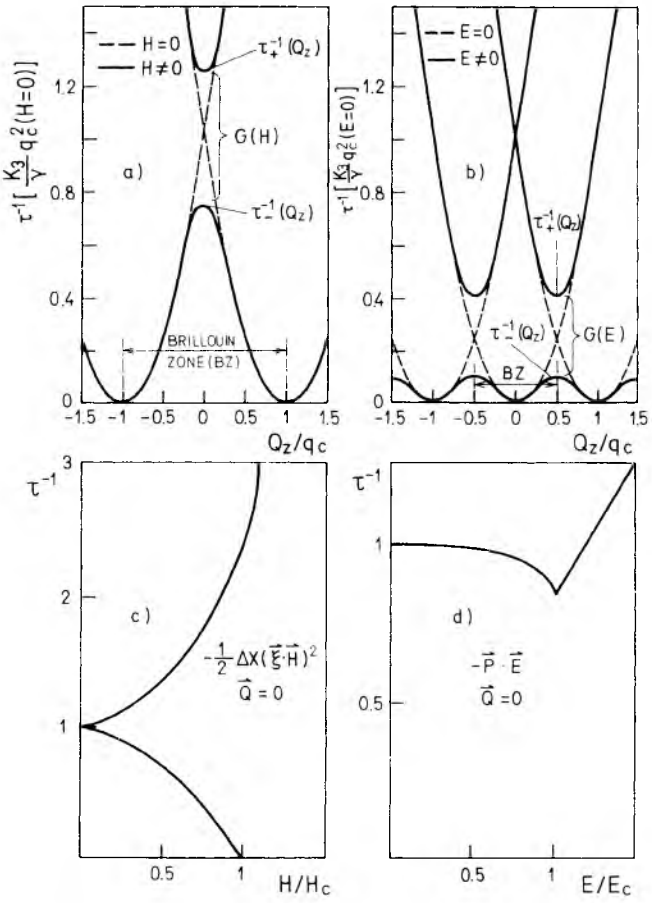

FIG. 10. Phason excitation spectrum in the case of the (a) diamagnetic and (b) ferroelectric couplings. The corresponding field dependencies of the relaxation rates at $\mathbf{Q}=0$ are shown in (c) and (d), respectively.

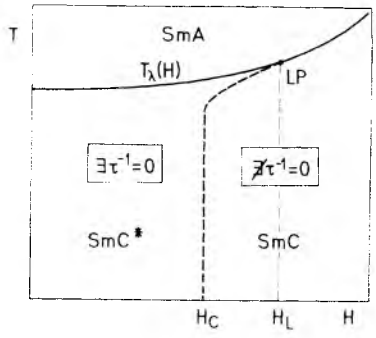

FIG. 11. The (H,T) phase diagram of a ferroelectric liquid crystal in an external magnetic field. The zero-frequency, symmetry-restoring Goldstone mode exists only in the region below $T_\lambda(H)$ and below the critical magnetic field $H_c(T)$.

and broken symmetry in a ferroelectric liquid crystal with a question, which is of particular interest: Is there some fundamental reason why the gapless, zero-frequency phason mode exists only below the critical field for helix unwinding, whereas it disappears as soon as the helix is unwound by the field? Since the existence of a gapless phason, which is here a zero-frequency, symmetry-restoring Goldstone mode, is related to the spontaneous symmetry breaking in the system, we have to consider the (H,T) phase diagram of a ferroelectric liquid crystal in an external magnetic field, which is shown in Fig. 11. If we neglect the periodic smectic layering, the Sm A phase has continuous translational symmetry, as well as the continuous D_∞ rotational symmetry, which can be spontaneously broken when the system is cooled across the second-order phase transition λ line, i.e., the T_λ (H) line. For $H=0$, the continuous translational symmetry of the Sm A phase is spontaneously broken by the appearance of the helical Sm C^* structure. In addition, the continuous D_∞ rotational symmetry is broken to a discrete C_2 symmetry. According to the Goldstone theorem,[2,3] a zero-frequency Goldstone mode should appear in the Sm C^* phase, as is indeed observed in the experiment. For $H\neq 0$, the field reduces the point symmetry of the Sm A phase to a discrete symmetry D_2, whereas the continuous translational symmetry of the Sm A phase is preserved. If the Sm A phase is cooled across the λ line at fields, lower than the Lifshitz field, $H<H_L$, as indicated in Fig. 11, the *continuous translation symmetry of the Sm A phase is broken* because of the appearance of π-soliton walls in a distorted Sm C^* phase. The Goldstone mode should thus exist, recovering the broken translation symmetry of the Sm A phase. On the contrary, if we cool the Sm A phase across the λ line at fields, higher than the Lifshitz field, $H>H_L$, only the *discrete point group of the Sm A phase is broken,* $D_2\rightarrow C_2$, whereas the continuous translation symmetry is preserved. The Goldstone mode should not exist at fields higher than the critical field, as is indeed observed.

VI. CONCLUSIONS

We have shown that the observed evolution of the band structure of the phason excitation spectrum in the Sm C^* phase in a transverse magnetic field can be very well understood on the grounds of simple symmetry arguments and similarities to other systems. In particular, these arguments show in a natural way the analogy between the dynamics of a phason excitation in a distorted Sm C^* phase and the motion of a particle in periodic crystal potential. The underlying mechanism, which is responsible for the similarity of both systems, is a breaking of a continuous symmetry. Whereas the magnetic field breaks the continuous helical symmetry of a perfect, undistorted Sm C^* structure by the creation of π-soliton walls, the periodic crystal lattice potential breaks the continuous translational symmetry. In contrast to the motion of a particle in a crystal lattice, the magnitude of the solitonlike deformation in a ferroelectric liquid crystal can be easily controlled by the magnitude of the external magnetic field at any given temperature.

[1]R. Blinc and B. Žekš, Phys. Rev. A **18**, 740 (1978).
[2]J. Goldstone, A. Salam, and S. Weinberg, Phys. Rev. **127**, 965 (1962).
[3]R. V. Lange, Phys. Rev. **146**, 301 (1966); see also D. Forster, *Hydrodynamic Fluctuations, Broken Symmetry, and Correlation Functions,* Frontiers in Physics, Lecture Note Series 47 (Benjamin, Reading, MA, 1975).
[4]I. Muševič, R. Blinc, B. Žekš, C. Filipič, M. Čopič, A. Seppen, P. Wyder, and A. Levanyuk, Phys. Rev. Lett. **60**, 1530 (1988).
[5]I. Drevenšek, I. Muševič, and M. Čopič, Phys. Rev. A **41**, 923 (1990).
[6]A. Levstik, T. Carlsson, C. Filipič, I. Levstik, and B. Žekš, Phys. Rev. A **35**, 3527 (1987); A. Levstik, Z. Kutnjak, C. Filipič, I. Levstik, Z. Bregar, B. Žekš, and T. Carlsson, *ibid.* **42**, 2204 (1990).
[7]I. Muševič, B. Žekš, R. Blinc, H. A. Wierenga, and Th. Rasing, Phys. Rev. Lett. **68**, 1850 (1992).
[8]B. Sutherland, Phys. Rev. A **8**, 2514 (1973).
[9]C. Fan, L. Kramer, and M. J. Stephen, Phys. Rev. A **2**, 2482 (1970).
[10]J. D. Parsons and C. F. Hayes, Phys. Rev. A **9**, 2652 (1974).
[11]M. Yamashita, H. Kimura, and H. Nakano, Prog. Theor. Phys. **65**, 1504 (1981).
[12]S. A. Pikin and V. L. Indenbom, Usp. Fiz. Nauk **125**, 251 (1978) [Sov. Phys. Usp. **21**, 487 (1978)]; R. Blinc, I. Muševič, B. Žekš, and A. Seppen, Phys. Scr. T **35**, 38 (1991).
[13]A. L. Fetter and M. J. Stephen, Phys. Rev. **168**, 475 (1968).
[14]J. Kay and H. E. Moses, J. Appl. Phys. **27**, 1503 (1956).
[15]W. L. McMillan, Phys. Rev. B **16**, 4655 (1977).
[16]A. D. Bruce and R. A. Cowley, J. Phys. C **11**, 3609 (1978).
[17]P. Bak, Phys. Rev. B **21**, 3287 (1980).
[18]P. Bak, Rep. Prog. Phys. **45**, 587 (1982).
[19]M. Horioka and A. Sawada, Ferroelectric **66**, 303 (1986).
[20]E. T. Whittaker and G. N. Watson, *Modern Analysis* (Cambridge University Press, Cambridge, England, 1935).
[21]P. Byrd and M. D. Friedman, *Handbook of Elliptic Integrals for Engineers and Physicists* (Springer-Verlag, Berlin, 1954).
[22]R. Pindak, *Solitons in Liquid Crystals,* edited by L. Lam and J. Prost (Springer-Verlag, Berlin, 1991), Chap. 7.
[23]C. Oldano, Phys. Rev. Lett. **53**, 2413 (1984).
[24]W. Kuczyński, B. Stryla, J. Hoffmann, and J. Malecki, Mol. Cryst. Liq. Cryst. **192**, 301 (1990).
[25]S. Garrof, R. B. Meyer, and R. Barakat, J. Opt. Soc. Am. **68**, 1217 (1978).
[26]O. Hudak, J. Phys. (Paris) **44**, 57 (1983); J. Phys. C **16**, 2659 (1983).
[27]J. Pavel, M. Glogarova, and S. S. Bawa, Ferroelectrics **76**, 221 (1987).
[28]J. Pavel and M. Glogarova, Ferroelectrics **121**, 45 (1991).
[29]B. Urbanc-Kutnjak, Ph.D. thesis, University of Ljubljana, 1993.

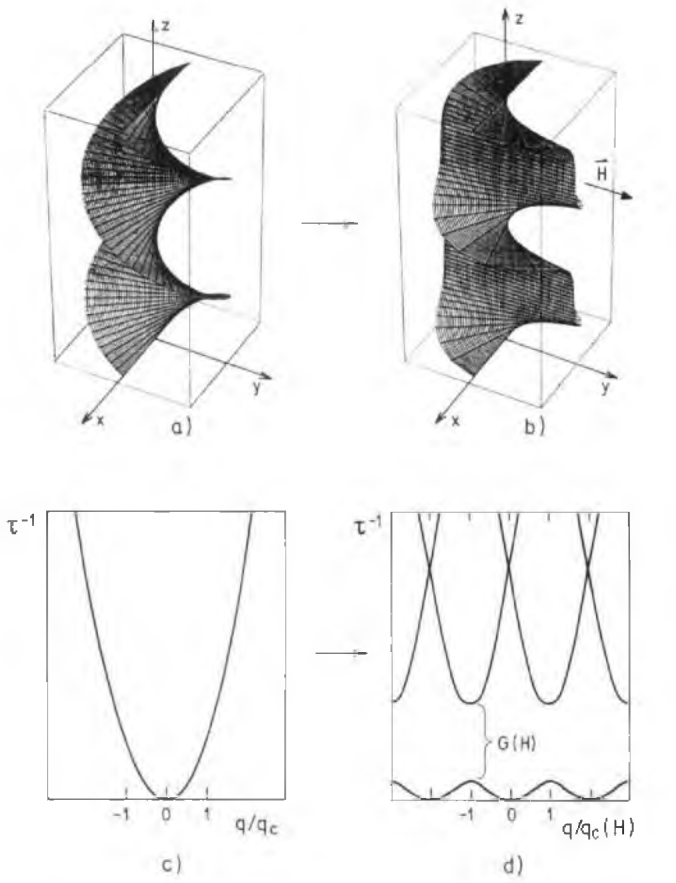

FIG. 1. The projection $\xi(z)$ of the director field on to the smectic layers for (a) $H=0$ and (b) $H \approx H_c$, as calculated from the Eqs. (1) and (3). In zero field, the unperturbed helical surface has a continuous helical symmetry as shown in (a). For $H \neq 0$ the distorted helical surface shows a discrete translational symmetry as shown in (b). (c) shows the phason dispersion in the unperturbed Sm C^* phase, whereas (d) shows schematically the phason dispersion in a solitonlike deformed Sm C^* phase.

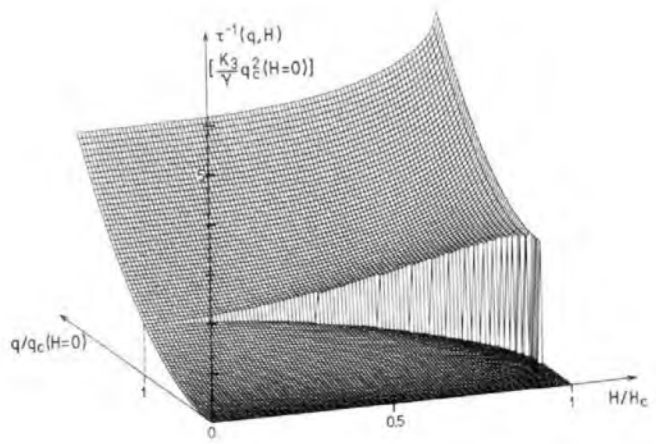

FIG. 5. 3D view of a calculated phason dispersion $\tau^{-1}(q,H)$ as a function of an external field. Note the appearance of a gap near q_c already at very small fields. Because of the numerical discreteness in H, the shrinking of the BZ near H_c is not complete.